Supplementary Information:

Harnessing Thermal Fluctuations for Purposeful Activities: The Manipulation of Single Micro-swimmers by Adaptive Photon Nudging

Bian Qian,[a‡] Daniel Montiel,[a] Andreas Bregulla,[b] Frank Cichos,[b] and Haw Yang*[a]

Computer Simulation Details

Using Eqs. (1) and (2) in the main text, one can numerically implement and test the proposed control algorithm for a photon-nudged particle. For simplicity, the buoyancy/gravitation force and the radiation-pressure force are removed from the motion equation (1) in the main text in all simulations because both buoyancy/gravitation force and radiation-pressure force add an additional layer of complexity for the controllability in z. In experiment, these two terms can be removed by proper experimental configuration, *e. g.*, counter-propagating laser beams, confined control motion on the xy plane (buoyancy/gravitation force and radiation-pressure force only function in $\hat{z}$) or matching between buoyancy/gravitation force and radiation-pressure force. With this arrangement, Eq. (1) in the main text reduces to

$$\dot{\mathbf{X}}(t) \quad = \quad U_{\rm th}(t)\hat{\mathbf{n}}(t) + \boldsymbol{\xi}(t). \tag{S1}$$

To represent the adaptive steering in our control algorithm, the value of $U_{\rm th}(t)$ is updated based on $\mathbf{r}(t)$ and $\hat{\mathbf{n}}(t)$ for each time step Δt in the simulation. Specifically, when the angle θ between $\hat{\mathbf{n}}$ and $\mathbf{r}$ is greater than a threshold, $\theta \geq \theta_t$, a laser is triggered to propel the micro-swimmer and correspondingly $U_{\rm th}$ = constant for finite laser power input. Otherwise, the micro-swimmer is left alone with the laser off, $U_{\rm th} = 0$. Note that we have performed two sets of simulations: 2D and 3D. Although for both simulations the particle motions are fully solved in three dimensional space, in 2D simulation the angle θ is measured on the $x-y$ plane while for 3D simulation θ is an angle in a three dimensional space. In another words, in 2D simulation only the particle motion on the $x-y$ plane is controlled. The 2D simulation is performed to reproduce the motion-control experiment for the comparison with experimental measurements.

Calculation of the Radiation-Pressure Force

Every single ray of light within the laser cone was assumed to be normal incident onto Janus swimmer surface. A ray of light exerts a force F to the particle as it impinges on the swimmer surface as illustrated in Fig. S1(a). Thanks to symmetry of the Janus swimmer, only the force components parallel to the optical axis, F_z, contribute to a net particle motion whereas the transverse components cancel out. For a ray of power P with a angle α to the optical axis z, $F_z = (2R + A)\frac{n_m}{c} P\cos\alpha$, in which $n_m = 1.413$ is the refraction index of surrounding medium (60% glycerol/water w/w), c the speed of light in vacuum, R and A the reflected and absorbed light power by the swimmer, respectively (cf. Fig. 2 in the man text).

[a] *225A Frick Chemistry Laboratory, Princeton University, Princeton, New Jersey 08544, USA. Fax: +1 609 258 3708; Tel: +1 609 258 3578; E-mail: hawyang@princeton.edu*

[b] *Molecular Nanophotonics, University of Leipzig, 04103 Leipzig, Germany.*

‡ Current address: Mechanical Engineering, Massachusetts Institute of Technology, 77 Massachusetts Avenue, Building3-264, Cambridge, Massachusetts 02139

For a Gaussian input laser beam, the power intensity of light drops exponentially from the center of the beam, $I_0 \exp[-\frac{2r^2}{w_0^2}]$, in which I_0 is the peak power intensity, r the transverse distance to the center of the laser beam, and w_0 the beam size. For a laser beam of power P_0, $I_0 = P_0/(0.5\pi w_0^2(1-e^{-2}))$. That is, the power carried by a single ray emanating from an unit area of a Gaussian beam is

$$P_0(0.5\pi w_0^2(1-e^{-2}))^{-1} \exp[-2\frac{r^2}{w_0^2}] r dr d\phi$$

After the microscope objective, treated as a single focusing lens here in the ray-tracing approximation (Fig. S1(b)), the rays are refracted and converged into a point.

By integrating the light energy from all rays within the laser beam, the propulsion force induced by laser irradiation can be determined,

$$F_z = (2R+A)\int_0^{2\pi}\int_0^{w_0} I_0 \exp[-2\frac{r^2}{w_0^2}]\cos\alpha r dr d\phi \quad \text{(S2)}$$

$$= 2\pi(2R+A)\int_0^{\alpha_{\max}} d\alpha I_0 \exp[-2\frac{(\ell_{\text{eff}}\tan\alpha)^2}{w_0^2}](\ell_{\text{eff}}\tan\alpha)(\ell_{\text{eff}}\sec^2\alpha)\cos\alpha, \quad \text{(S3)}$$

where ℓ_{eff} is the effective focal length of the microscope objective and $\alpha_{\max}$ is the maximum cone angle defined by the experimental numerical aperture when a variable NA objective is used as in the present case. Note the Jacobian term, $\ell_{\text{eff}}\sec^2\alpha$, when changing the integration from dr to $d\alpha$. The ℓ_{eff} can be estimated by the back aperture of the objective (7 mm for the present case) and the full numerical aperture (NA = 1.4, oil immersion with $n_{\text{oil}} = 1.4790$). In the experiment, the beam diameter is about 5 mm ($w_0 = 2.5$ mm) at NA = 0.7. With these experimental parameters, the radiation-pressure force on the particle can be estimated as reported in the main text.

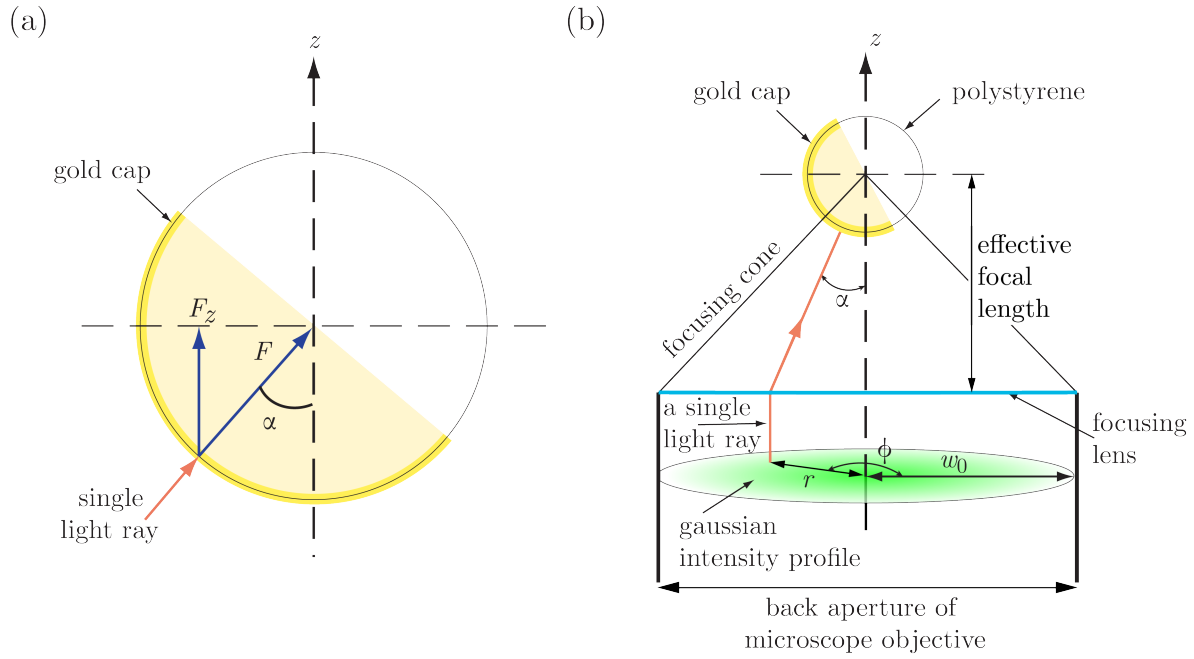

Figure S1 (a) Illustration of irradiation force on the particle exerted by a single ray of laser light. (b) The ray-tracing model used to calculate the radiation-pressure forces.

Reconstruction of Particle Orientation

The difference in refraction index causes a variation in the amount of light scattering between gold cap and polystyrene particle surface. Due to this difference in light scattering, the capped particle under dark-field

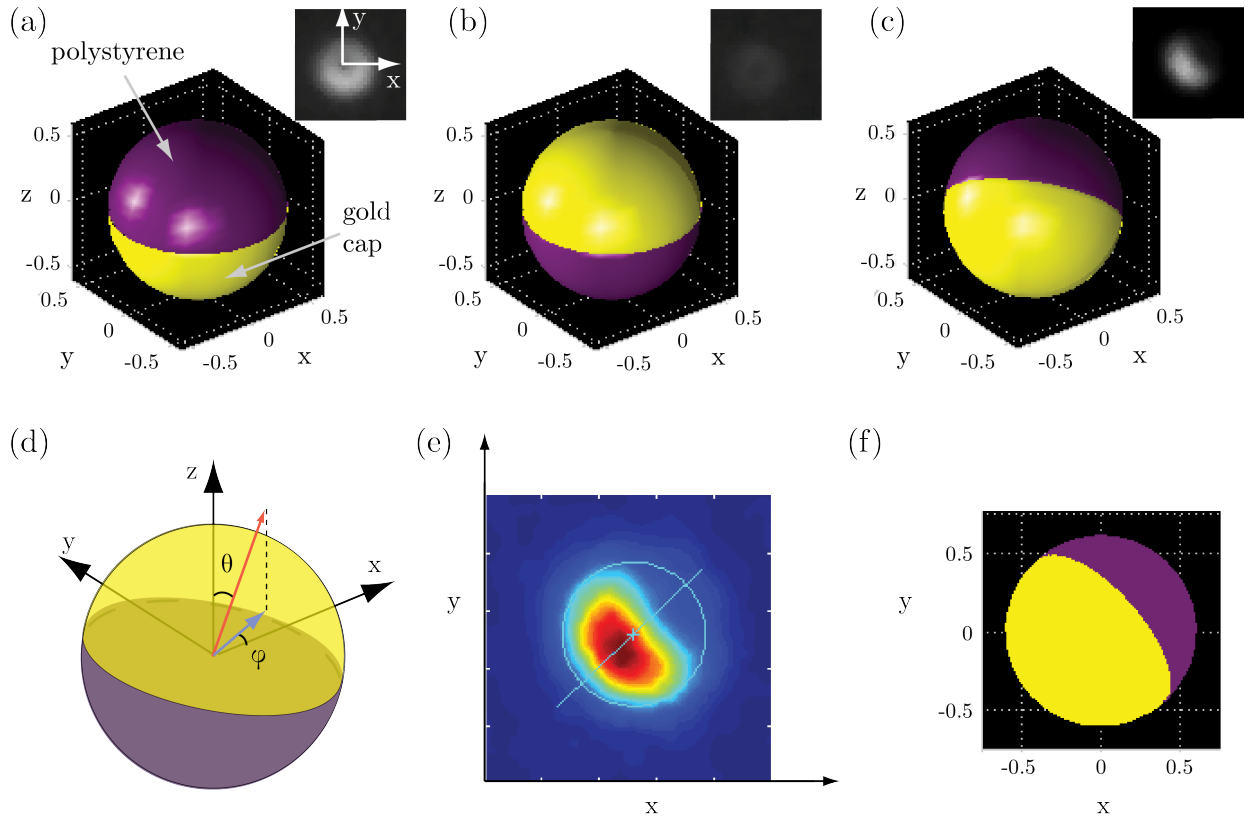

Figure S2 (a)(b)(c) Dark-field images of a capped particles at different orientations and their 3D representations on a Cartesian coordinate. The coordinate origin locates at the center of the particle. Axis z is set along the direction of laser propagation. The collecting microscope objective is placed on a −z plane. (d) Illustration of the angles used to determine the three dimensional orientation of the particle. The red arrow represents the particle axis, pointing from polystyrene to gold. The blue arrow is the projection of particle axis on the x-y plane (image plane). (e) Determination of the in-plane particle orientation from the image of the particle in (c). The circle represents the convolution window used for searching the particle center. The cross within the circle denotes the found particle center on the image. The line is the searched particle axis which bisects the brightness within the circle. (f) Projection of a capped particle orienting at $\theta = 115.3°$,$\phi = 228.5°$ on the image plane. The total image brightness of a particle at specific orientation was estimated by convolving the particle projection with the intensity profile of that of gold-cap end facing −z, as in (a), and that of the polystyrene end facing −z, as in (b).

illumination appears as a moon-like feature on the image, as shown in Fig. S2(a)-(c). The bright region of the moon-like feature corresponds to the gold cap whereas the polystyrene portion is barely visible because its refraction index is close to that of glycerin. For each image a MATLAB program was used to subtract out the background. After background removal, the image was convolved with a circular window the size of which was the same as that of the particle on the image. The brightest point on the convolved image corresponds to the particle center. Having located the particle center on the image, the particle orientation can be determined by finding its axial symmetric axis. As defined in Fig. S2(d), the particle axis points from polystyrene to gold cap. The projection of the particle axis on the image plane, the ϕ angle, was obtained by finding the line that both bisected the brightness of the particle image and went through the particle center (Fig. S2(e)). Determining the projection of the particle axis on the plane perpendicular to the image plane was not trivial, however. Considering that the brightness of the particle image depended on the amount of gold and polystyrene seen by the observer, the out-of-plane axial orientation, θ, was obtained by calculating the ratio of gold/polystyrene on the particle surface facing the objective (Fig. S2(f)). To obtain the correct gold/polystyrene ratio, the image intensity profile of a complete gold cap (Fig. S2(a)) and a whole polystyrene bead (Fig. S2(b)) must be known beforehand. For sufficiently long movies consisted of consecutive time series of images, fortunately, it was easy to find the particle images under such conditions. In

other words, the intensity profiles are calibrated *in situ* such that potential particle-to-particle variations do not pose an issue. Having known both in-plane and out-of-plane axial orientations, the particle axisymmetric axis in the three-dimensional space can be uniquely determined.